Research Article

Ronghui Zhang, Cong Liu, Wanting Gou, and Qiang Liu*

Comprehensive performance analysis and optimal design of smart light pole for cooperative vehicle infrastructure system

https://doi.org/10.1515/ntrev-2021-0061
received June 25, 2021; accepted July 27, 2021

Abstract: On the basis of the finite element theory, in this study, a theoretical design and simulation practice to carry out steady-state static analysis, structural dynamics analysis, and electromagnetic interference characteristics analysis on smart light poles, is combined. On this basis, a design of modular weight reduction and cost reduction was proposed, which realized the multi-objective parameter optimization of the smart light pole. The simulation results show that the mass of the optimized light pole can be reduced by 14.2%, and the material cost can be reduced by 14.7%. At the same time, the comprehensive performance of the optimized smart light pole can still meet the design requirements of the industry standards. The research results provide a reference for the lightweight design and the comprehensive analysis of the smart light pole in the future.

Keywords: the smart pole, the finite element theory, steady-state static analysis, dynamics analysis, electromagnetic interference, cost reduction, lightweight technology design

1 Introduction

With the construction and development of smart cities, smart light poles will be one of the important and dense elements in infrastructure construction [1]. The smart light pole has the characteristics of multi-pole integration and rich equipment [2]. Through function superimposition and port reservation, it can integrate smart lighting, weather station, AP (Wireless Access Point) equipment, SOS pager used as emergency call system, and charging pile. It is not only a technical integration but also an innovation in management mechanism. It is an effective support for the improvement of urban governance efficiency [3]. In the vehicle–road collaborative system, the smart light pole is the carrier of the roadside, which is responsible for the data collection and information release in the perception layer of the Internet of Things. Through 5G communication, real-time intercommunication and interconnection of vehicle units are realized to meet the needs of vehicle–road coordination [4].

As the 5G communication technology was experimentally researched and demonstrated in China, major operators have carried out corresponding research and application projects. In 2021, social services related to 5G communication technology have gradually entered people's daily life. Therefore, in order to further enhance the mobile communication network coverage of urban communications, smart light poles widely distributed are an important and perfect carrier. At the same time, the in-depth integration of smart light poles and 5G communication technology will be an important development trend.

The promotion and application of smart light poles is still in its infancy, and there is still room for improvement in structural design. An earthquake may cause serious damage to the smart light pole as it is a steel structure building, so seismic performance is important. However, scholars usually only perform steady-state static analysis and modal analysis when checking the comprehensive performance of light poles. In contrast, compared with traditional light poles (Figure 1), there are more electronic devices mounted on smart light poles. And electronic devices are prone to electromagnetic interference with each other. To meet the performance requirements, finite element analysis and lightweight design work are still rarely carried out at this stage. Therefore, the actual

* **Corresponding author: Qiang Liu,** Guangdong Key Laboratory of Intelligent Transportation System, School of Intelligent Systems Engineering, Sun Yat-Sen University, Guangdong 510275, People's Republic of China, e-mail: liuq32@mail.sysu.edu.cn
Ronghui Zhang, Cong Liu, Wanting Gou: Guangdong Key Laboratory of Intelligent Transportation System, School of Intelligent Systems Engineering, Sun Yat-Sen University, Guangdong 510275, People's Republic of China

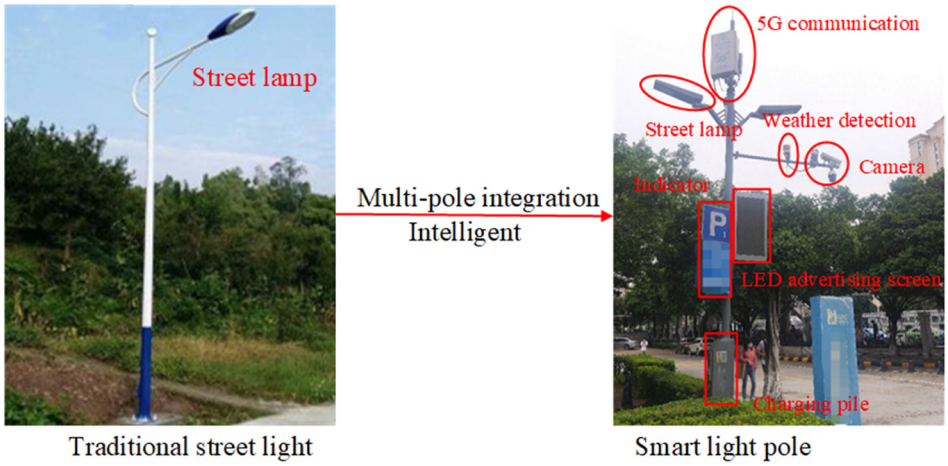

Figure 1: The difference between the smart light pole and the traditional light pole.

amount of materials for smart light poles is often relatively surplus, resulting in higher quality. In addition, when the light pole is damaged, the repairing method of the whole pole replacement is too expensive, and the cost of the pole itself is also relatively high. Insufficiencies such as heavy quality and high cost will greatly limit the development of the light pole industry. Therefore, it is important to study the comprehensive performance of smart light poles and the scheme of reducing weight and cost. It will benefit the construction and promotion of smart light poles.

In this study, the following research are carried out in response to the aforementioned problems. First of all, in addition to steady-state statics analysis, this study further conducted seismic analysis on the light pole based on modal analysis to study how to ensure that it has sufficient seismic capacity in earthquakes. Second, in this study the electromagnetic radiation interference of smart light poles was innovatively analyzed, and the mutual electromagnetic interference between the mounted electronic devices was checked. Third, an optimized design for weight reduction and cost reduction was made for the smart light pole, and the comprehensive performance of the optimized smart light pole was checked, which verified the feasibility of the solution.

1.1 Literature review

For solar street lights, high-pole lights, and ordinary street lights, scholars have conducted many kinds of research. With the help of the finite element software [5–10], they carried out design calculations and mechanical performance verification on light poles under specific conditions, obtained the structural characteristics, and verified the rationality of the design scheme. For example, Soltani *et al.* [11] analyzed the structure of the hexagonal wind-resistant light pole and further evaluated the reliability of the light pole. Ai *et al.* [12] conducted a finite element analysis on the smart light pole and carried out performance test, damage test, and exploration of the prevention method. Zajac and Przybylek [10] studied the diagnosis and prevention of the street light pole damage, established a finite element model, and obtained the method to reduce the damage of the pole through calculation and analysis. The improved results have been tested to prove the method effectiveness. Zhang [13] used the finite element software ANSYS to analyze the pole structure and designed a cone-shaped hexagonal lamp, whose material used was precipitated calcium carbonate. The simulation results have verified that the load and the maximum stress of the light pole were reduced, which proved design reliability. Pal *et al.* [14] studied the galvanized poles for street lights. A finite element analysis was carried out, and it was observed that the high stress caused by the wind speed of 86 km/h exceeded the pole yield strength. Juric and Linden [15] mainly studied the stress cycle, failure, and the fatigue performance of the lamp pole connection under wind load and estimated the fatigue life of different locations. Solari and Pagnini [16] conducted analysis and experimental research on the street light pole under wind excitation. Without considering the amount of eccentricity, the wind vibration response and galloping behavior of street light poles with concentrated mass and different modes have been proved. Balagopal *et al.* [17] proposed a model that can predict the natural frequency and

displacement of the light pole structure. The results show that the longitudinal load will cause the horizontal second-order displacement of the light pole, and the predicted natural frequency is the same as the modal analysis results. Sun *et al.* [18] studied the stress on the rectangular light pole. By increasing the bolt pre-tightening force, the stability of the base flange was improved, and the displacement of the lamp pole was reduced. Furlane *et al.* [19] deduced the background response algorithm based on equivalent strain energy theory, and finally the method was applied to the equivalent static wind load analysis.

1.2 Methodology

Based on the finite element theory, we combined theoretical design and simulation practice to carry out steady-state static analysis, structural dynamics analysis, and electromagnetic interference characteristics analysis on smart light poles. And on this basis, we proposed multi-objective parameter optimization and conducted lightweight design of the smart light poles. The research results provide relatively complete technical solutions for the research and design of smart poles, which has engineering value and practical significance for the rod resource effective integration, smart light pole manufacture, and the mounting equipment rational layout.

In this study, the finite element model of the smart light pole is established in Section 2. The comprehensive performance analysis of smart light poles is conducted in Section 3. The lightweight design and cost optimization design of the smart light pole are done in Section 4. Conclusions and future perspectives are presented in Section 5.

2 Establishment of finite element model

As shown in Figure 2, in the cooperative vehicle infrastructure system (CVIS), the smart light pole is the key link between smart transportation and smart cities.

In order to reduce traffic costs, improve traffic efficiency, and ensure traffic safety, we are committed to design a lighter and lower cost smart light pole. We conducted the geometric modeling and structural optimization analysis on smart light poles, which are the roadside unit perception carriers.

With reference to the physical pictures of the mounted equipment and the main pole, the physical assembly relations of the smart light poles, and related standards, smart light poles are geometrically modeled by using the large-scale digital model software UG. And then the 3D model obtained is imported into the software HyperMesh. The finite element model of the smart light pole is established through steps such as mid-surface extraction, geometric simplification, mesh division, material setting, and connection simulation. The final model of the smart light pole is shown in Figure 3.

The material of the main pole is Q235, whose wall thickness is 3.5 mm. The parameters of the material are shown in Table 1. The relevant material properties and

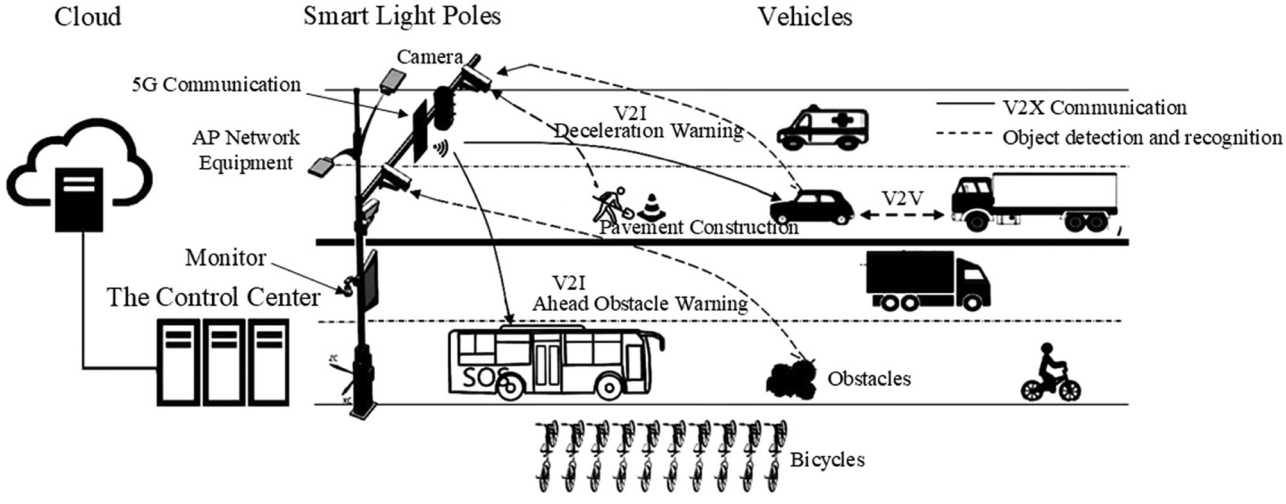

Figure 2: Application of smart light pole in CVIS.

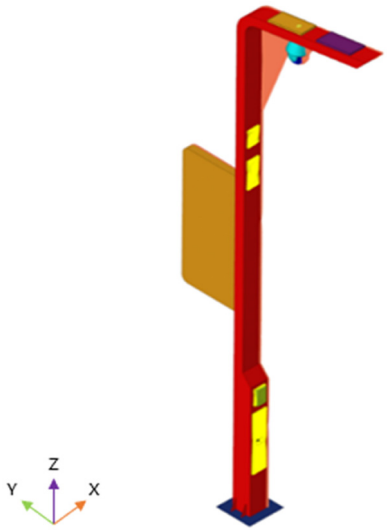

Figure 3: The final model of the smart pole.

physical properties need to be assigned accordingly into the finite element model of the smart light pole.

3 Comprehensive performance analysis of smart light poles

Through finite element simulation modeling, a simulation model of smart light poles based on steady-state statics, structural dynamics, and electromagnetics has been obtained. And then steady-state statics analysis, structural dynamics analysis, and electromagnetic interference analysis are carried out by using finite element simulation technology.

3.1 Steady-state static analysis

Smart light poles are usually located outdoors such as highways and streets. As a result, the working environment is harsh in most cases. They are often disturbed by various extreme weather and disasters such as typhoons, storms, ice, and snow. We used software HyperWorks to check the mechanical performance of smart light poles under full load conditions of typhoons, snow, and the combination of wind and snow.

3.1.1 Full load condition of typhoon

In the design and verification of smart light poles, the wind load impact must be fully considered. The wind load, which is equivalent to static force, is applied to the smart light pole based on the approximation principle. In the code named as *Load Code for the design of building structures* promulgated by China, the standard value of wind load is calculated by the following formula:

$$w_k = \beta_z \mu_S \mu_Z w_0, \quad (1)$$

where w_k is the standard value of wind load at altitude z, w_0 is the local basic wind pressure, μ_S is the wind load figure coefficient, μ_Z is the coefficient of wind pressure variation with height, and β_z is the wind vibration coefficient.

For smart light poles, the standard value of wind load at different heights is different. After comprehensive consideration, the smart light pole is divided into three sections, namely the bottom light pole, the middle light pole, and the upper light pole. According to each mounted device position, it is determined that the bottom pole height is 0–1.9 m, the middle pole height is 1.9–4.5 m, and the top pole height is 4.5–6 m. The specific situation is shown in Figure 4.

Refer to the relevant case and the regulation named as *Load code for the design of building structures GB50009-2012*, when typhoon conditions are applied, that the wind speed under the most dangerous condition and the wind direction when the windward area is the largest are selected. The maximum wind speed value of a level 12 typhoon is 36.9 m/s, and in the horizontal direction, the wind acts vertically on light emitting diode advertising screen. We apply the wind load as concentrate force respectively on the center of the three sections, the display screen, and the camera. And the specific situation is shown in Figure 4. The values of different wind load applied on different items are shown in Table 2.

3.1.2 Full load condition of snow

In order to obtain the finite element model under the full load condition of snow, in the form of a uniform load press, the snow load is applied vertically downwards

Table 1: Parameters of the main rod material

Name	Material	Elastic modulus (GPa)	Poisson ratio	Density (T/m^3)	Yield strength (MPa)
The main pole	Q235B	206	0.33	7.85	235

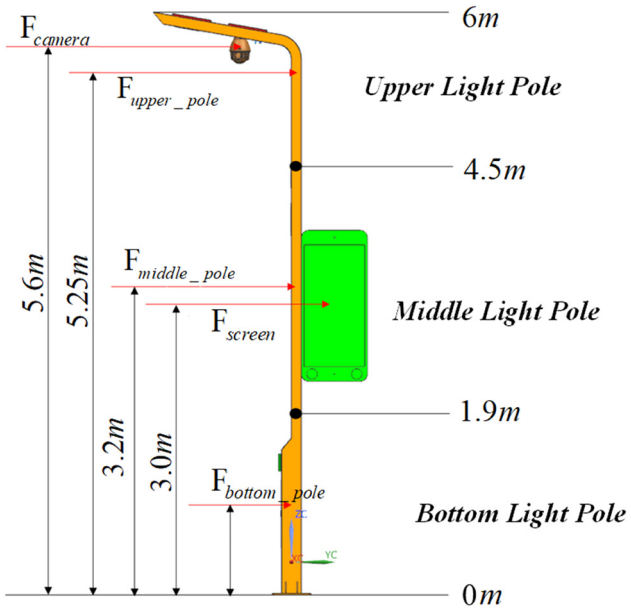

Figure 4: Schematic of the smart light pole subjected to wind load.

Table 2: Values of wind load

Parameters	Bottom light pole	Middle light pole	Upper light pole	Screen	Camera
h (m)	0.95	3.2	5.25	2.98	5.64
β_z	1.11	1.68	2.24	1.61	2.34
μ_z	0.49	0.71	0.82	0.70	0.84
w_k (kN/m^2)	0.28	0.61	0.94	17.00	1.00
S (m^2)	0.31	0.26	0.30	1.05	0.095
F (N)	86.80	158.60	282.00	598.50	95.00

on the top surface of the light pole crossbar and the top surface of the display screen. The value of the snow load is related to the amount of snowfall and the bearing area. According to the regulation named as *Load code for the design of Industrial and Civil building structures*, the snow load standard value is calculated by the following equation:

$$S_k = \mu_r S_0, \tag{2}$$

where S_k is the snow load standard value, S_0 is the basic snow pressure, and μ_r is the distribution coefficient of ice and snow.

3.1.3 Full load condition of wind and snow

In coastal areas abroad, snowstorms may occur. In this case, the wind load and snow load effects must be considered at the same time. The light pole is subjected to the horizontal concentrated load and the vertical uniform load at the same time, which is easy to cause the top crossbar and display screen to be damaged and fall off. That will greatly affect the light pole function. It is necessary to verify the light pole mechanical performance under the typhoon and snow superposed action. The authors create a new loadadd in the software HyperMesh, superpose the typhoon condition and the snow condition, and obtain the smart light pole finite element model under the combined condition of wind and snow.

3.1.4 Result of steady-state static analysis

The authors use the OptisTruct that comes from HyperWorks to carry out the modal simulating calculation, and the smart

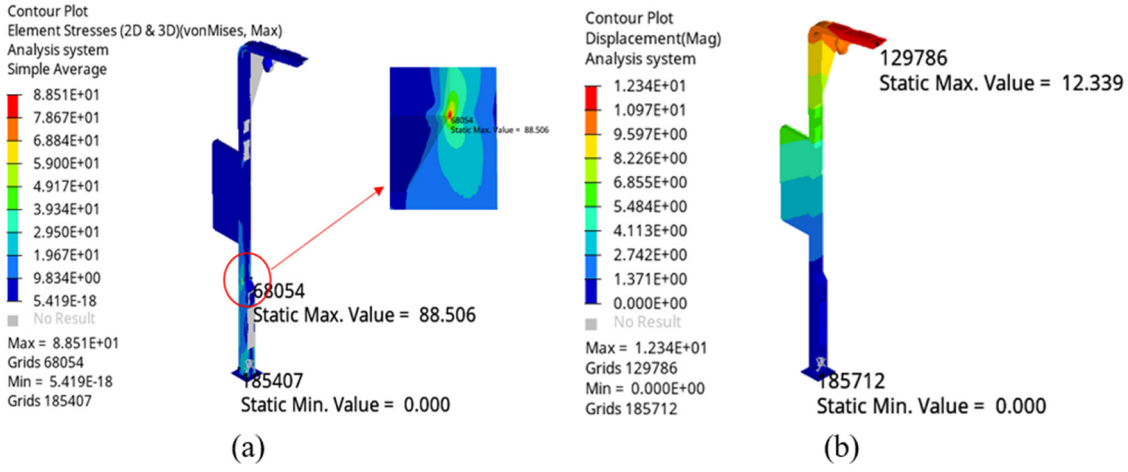

Figure 5: The cloud diagram under full load condition of typhoon: (a) stress and (b) displacement.

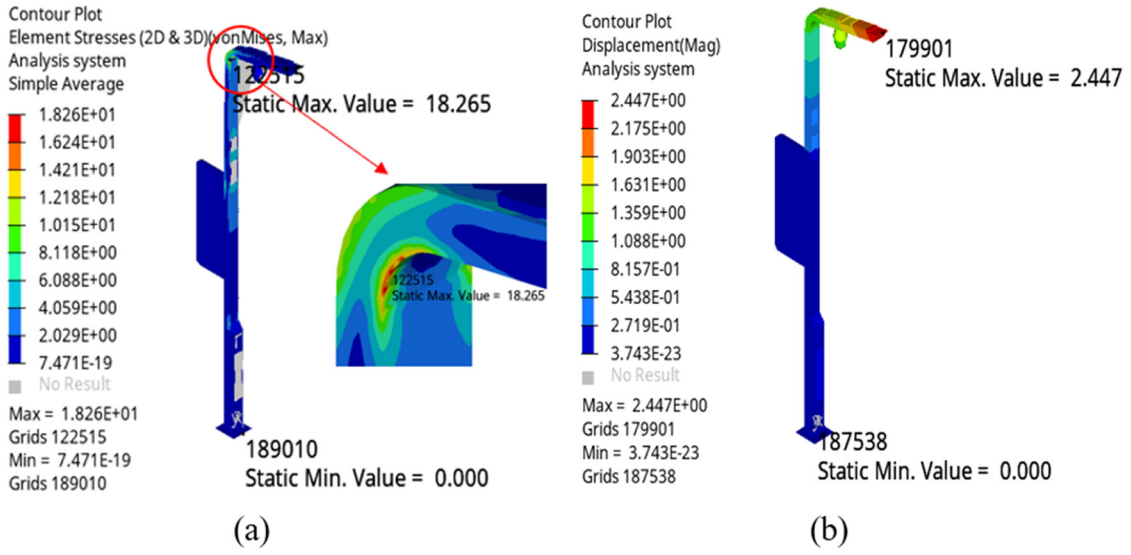

Figure 6: The cloud diagram under full load condition of snow: (a) stress and (b) displacement.

light pole cloud diagrams under the three extreme conditions are obtained, which are shown as follows (Figures 5–7).

Through the above finite element mechanical analysis, the smart light pole's steady-state mechanical analysis results are obtained, as shown in Table 3. The smart light pole's maximum stress and displacement under the three full load conditions are within the allowable range given by the standard, which conforms to the design requirements. Moreover, the maximum values of stress and displacement under the three extreme conditions are far less than the allowable value, indicating that the material amount for the smart light pole is too surplus, and the design can be optimized.

3.2 Structural dynamics analysis

The smart light pole modal analysis is helpful to provide important parameters for the seismic analysis [20]. According to the vibration natural frequency and mode, the smart light pole's weak part and dangerous structure

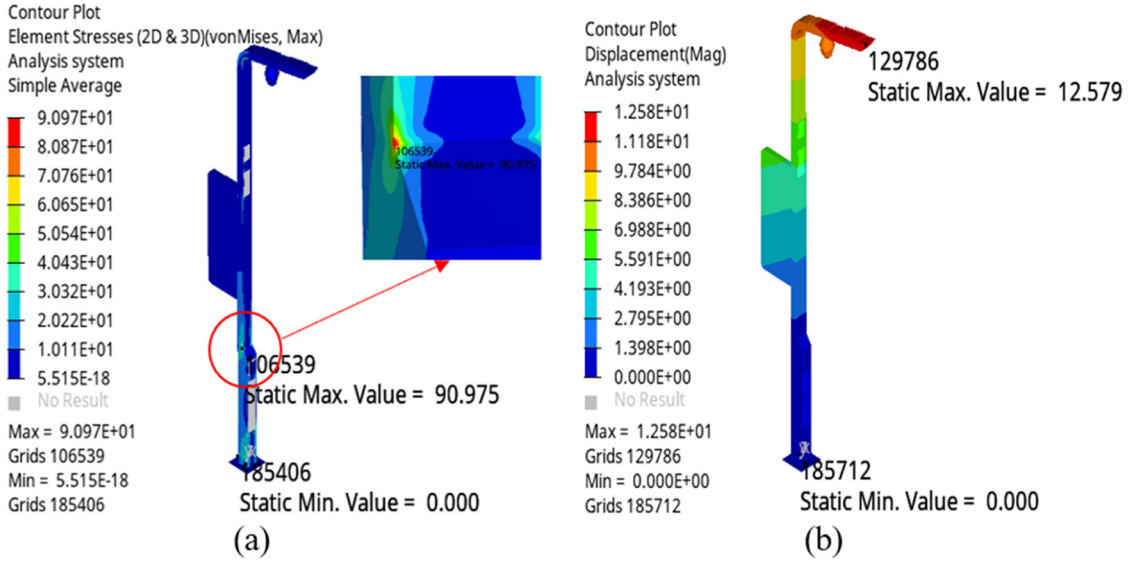

Figure 7: The cloud diagram under full load condition of wind and snow: (a) stress and (b) displacement.

Table 3: Steady-state mechanical analysis results of smart light poles

Condition	Analysis item	Result	Allowable value	Qualified (Y/N)
Full load of typhoon	Maximum stress	88.5 MPa	235 MPa	Y
	Maximum displacement	12.3 mm	150 mm	Y
Full load of snow	Maximum stress	18.3 MPa	235 MPa	Y
	Maximum displacement	2.4 mm	150 mm	Y
Full load of wind and snow	Maximum stress	91.0 MPa	235 MPa	Y
	Maximum displacement	12.6 mm	150 mm	Y

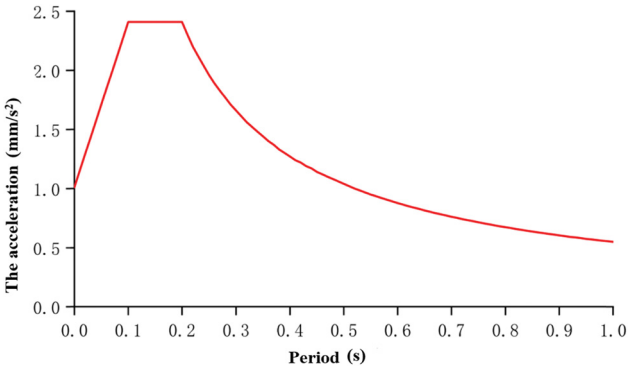

Figure 8: The seismic response spectrum curve.

can be found so as to provide reference for the subsequent optimization design.

We imported the previously established finite element model into HyperWorks. Without setting constraints, we conducted a free modal analysis on the smart light pole. The analysis results show that the smart light pole minimum natural frequency is 15.5 Hz and the maximum is 181.3 Hz. The frequency change between adjacent orders is relatively stable. Except for the slight weak connection between the main pole and the charging pile, the twelfth-order mode graph does not appear to be an obvious distortion.

3.2.1 Structural dynamics analysis under full load condition of earthquake

In the event of earthquakes, the main pole may collapse, structural parts are prone to damage, and the display screen is also easy to fall off, seriously affecting the pole's normal use. It is of great practical significance to study how to ensure that it has sufficient seismic resistance in earthquakes [21].

According to the regulation named as *Specification for design and engineering of construction of multi-function smart pole system*, we set the seismic response spectrum parameters of smart light poles as follows. The degree of the seismic fortification intensity is 7, and basic seismic acceleration value is set to 0.15 g. Besides, according to the regulation named as *GB 50011-2010 Code for Seismic Design of Buildings* (*2016*), the characteristic period is set to 0.2 s, the structural damping ratio is 0.04, and the response spectrum amplification factor of the Class II site is 2.25. Based on the above parameter setting, the seismic response spectrum curve can be obtained by the China Earthquake Code Response Spectrum Generator, as shown in Figure 8. This curve can better reflect the vertical acceleration periodic changes when an earthquake occurs.

We exported the response spectrum data table through the response spectrum curve, and then imported this table to HyperWorks. At the same time, we set constraints to all of six freedom degrees and conducted seismic analysis on the smart light pole. In order to verify whether the smart light pole meets the seismic response spectrum design requirements, the modal analysis results are linked with the determined response spectrum to calculate the model stress and displacement [22].

After the simulation calculation, the simulation results are obtained. The stress and strain results under the earthquake action can be viewed in the post-processor HyperView. The smart light pole cloud diagram under the earthquake's full load condition is shown in Figure 9.

According to Figure 9, the smart light pole's maximum displacement under the earthquake action is 1.74 mm, which appears at the tip of the top crossbar. It is clear that the deformation is small and meets the standard requirements. The maximum stress is 343.14 MPa, which appears at the junction of the bottom flange and the main rod. This value is greater than the yield strength of Q235B, indicating that there exists stress concentration in the structure. Unfortunately, this does not meet design requirements. As a result, in the subsequent optimization design, the corresponding plate thickness should be increased, or the bottom flange material should be replaced.

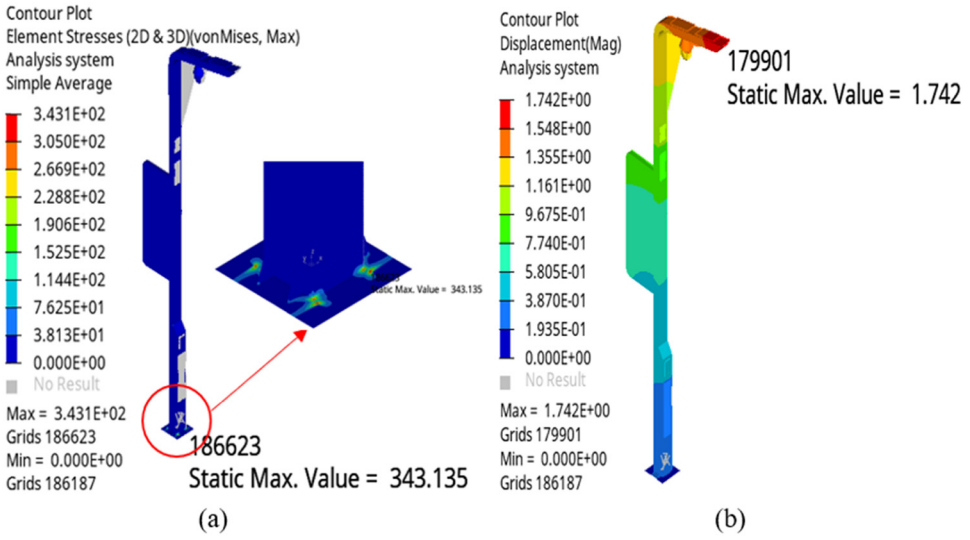

Figure 9: The cloud diagram of the smart light pole under the full-loaded seismic condition: (a) stress and (b) displacement.

3.2.2 Result of structural dynamic analysis

We conducted the structural dynamics analysis on smart light poles, explored the mechanical properties of light poles under varying loads, and analyzed whether the original light pole meets the design requirements. The results are shown in Table 4.

The analysis results show that the maximum displacement of the smart light pole structure under the earthquake condition is 1.74 mm, which meets the requirements of the standard. However, the maximum stress is 343.1 MPa, which exceeds the allowable value. The corresponding plate's thickness should be increased or the bottom flange material should be replaced in the subsequent optimization design.

3.3 Electromagnetic interference characteristics analysis

There are many electronic devices mounted on smart light poles. So it is necessary to determine the electromagnetic radiation source and conduct electromagnetic radiation interference analysis on smart light poles [23].

Table 4: Results of smart light poles under the seismic condition

Condition	Analysis item	Result	Allowable value
Full loaded of seismicity	Maximum stress Maximum displacement	343.1 MPa 1.74 mm	235 MPa 150 mm

3.3.1 Electromagnetic simulation modeling and calculation

In this study, we used ANSYS Electronics Desktop to numerically calculate the smart light pole model's electromagnetic radiation and interference. After the numerical calculation of the electromagnetic field, the electromagnetic field distribution is shown in Figure 10.

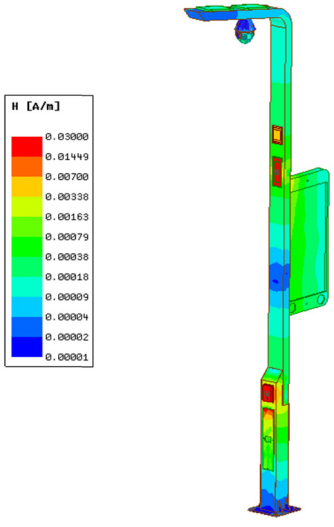

Figure 10: The cloud diagram of the magnetic field intensity distribution of the overall device.

The result of the electromagnetic simulation analysis shows that AP equipment and SOS pager both are radiation sources. The color of AP and SOS in the cloud diagram is dark red, which means their magnetic field strength is greater. And the rest of the mounted devices are basically blue or green, indicating that the magnetic field intensity emitted by the radiation source to other devices is low. Namely, the electromagnetic interference generated is very weak.

There exist electromagnetic emission sources in AP and SOS, resulting in higher magnetic field strength near the installation location. The farther away from these two devices, the less intense radiation of the magnetic field is received, which conforms to the fundamental principle of electromagnetic radiation. Moreover, for other adjacent devices, the intensity of the magnetic field emitted by the two radiation sources is low, which is not enough to generate strong electromagnetic interference.

As shown in Figure 11, because the main pole material Q235 has electromagnetic wave shielding characteristics, the magnetic field on the back of the main pole is weaker than that on the front, and the display screen is less interfered.

From the magnetic field line on the graph, it can be seen that the magnetic field strength decreases rapidly as the distance from the emitter increases. And the magnetic field strength of SOS is higher than that of AP. In order to learn the interference of the device SOS to the AP equipment, this study calculates the coupling coefficient between AP and SOS. After calculation, the result shows that the coupling coefficient between the two is only 0.02%, which means they are ultra-low coupling and not enough to produce strong interference.

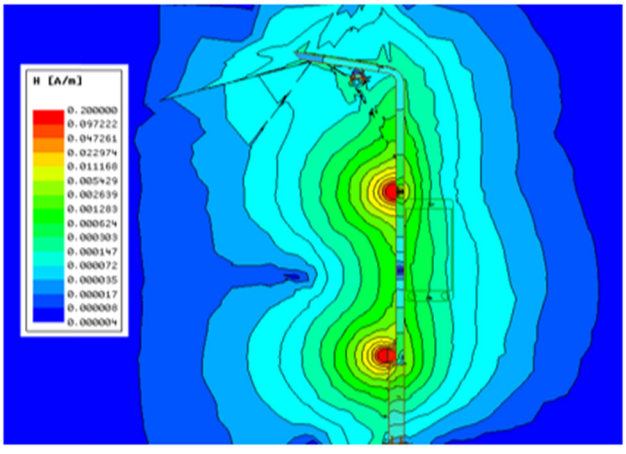

Figure 11: The top view of electromagnetic field radiation section.

3.3.2 Conclusion of electromagnetic simulation analysis

Maxwell software was used to carry out the electromagnetic field simulation on the smart light pole. The calculation result shows that when SOS and AP work at the same time, a certain amount of electromagnetic waves will be emitted into the space, causing a certain amount of electromagnetic interference to adjacent devices. Through the quantitative calculation of the electromagnetic field, it is found that the radiated magnetic field intensity between adjacent devices is very low, and the interference to adjacent devices is so weak that can be ignored. Through the calculation of the coupling coefficient, it is indicated that the interference between AP and SOS is very low, and there is no obvious electromagnetic interference condition.

4 Optimal design of smart light pole

From results of the comprehensive performance analysis, it can be seen that the maximum stress and displacement of the smart light pole, under the three extreme conditions, are far less than the allowable value given by the standard. It is indicated that the material amount is too surplus, and there is a large amount of room for optimization design. So it is very important to explore a more reasonable and lower-cost optimization plan for the large-scale promotion and application of smart light poles.

4.1 Multi-parameter sensitivity analysis

Before optimizing the design, it is necessary to perform sensitivity analysis on the model [24]. In this study, we innovatively used hammersley [25] in the sensitivity analysis. It is suitable for multi-factor analysis, can achieve hundreds of matrix operations, and can obtain sampling results relatively quickly.

According to the principle of symmetry and coplanarity, the main pole is divided into ten groups of sheet metal parts. The wall thickness of each group is used as the size variable, and the elastic modulus is used as the material variable. There are a total of 20 design variables. A multi-parameter sensitivity analysis model for the smart light pole has been established [26–30], as shown in Figure 12.

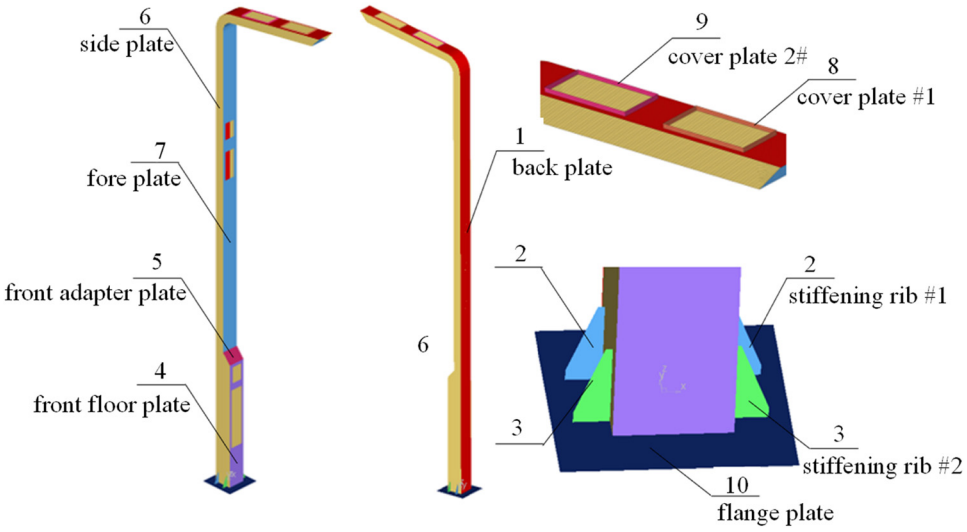

Figure 12: The grouping diagram of smart light pole parts.

Taking the mass minimization as the optimization goal, we used the software HyperStudy to calculate the established sensitivity analysis model. The result of the mass parameter sensitivity analysis is shown in Figure 13. The design variables in the figure are positively related to the mass. In order to minimize the mass of the smart light pole, the values of gan5.T.1, gan1.T.1, and gan7.T.1 should be reduced for the optimization design.

It can be seen from Figure 14 that design variables in the figure are negatively related to the maximum stress. In order to achieve the maximum stress value to be not greater than the initial value, the parameter values of gan1.T.1, steel10.E, and steel1.E should be increased or kept unchanged when optimizing the design. As shown in Figure 15, the design variables are negatively related to the maximum displacement as well. Therefore, it should also consider increasing or keeping the parameter values of gan1.T.1, gan5.T.1, and gan10.T.1 when optimizing the design.

4.2 Joint optimization of materials and sizes

In view of the fact that the smart light poles' mechanical properties under extreme conditions far meet the design standards' requirements, one can make the structural performance and material consumption of the light pole to be optimized through the reasonable combination of key design variables such as sizes and materials.

The joint optimization of sizes and materials still uses the design variables in the sensitivity analysis model. By

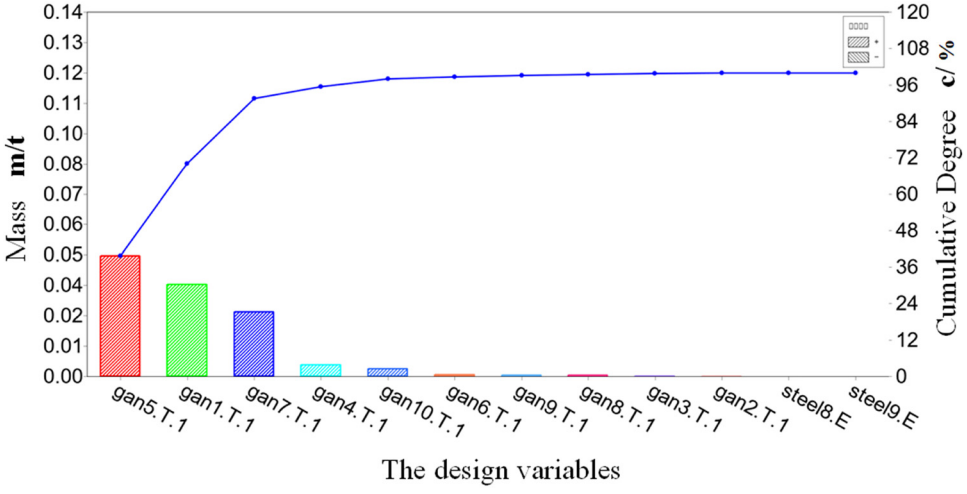

Figure 13: The result of the sensitivity analysis for mass parameters.

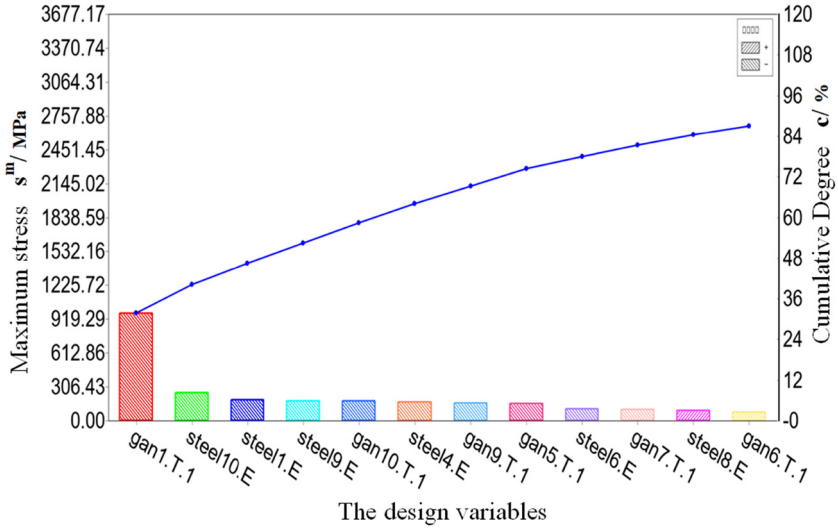

Figure 14: The result of the sensitivity analysis with stress parameters under wind and snow conditions.

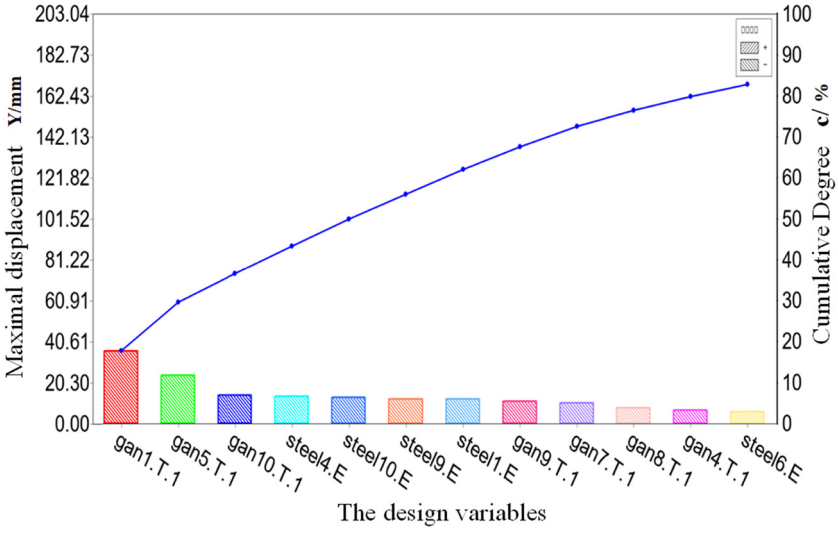

Figure 15: The result of the sensitivity analysis with displacement parameters under wind and snow conditions.

using OptisTruct, the mass curve converges and tends to be minimized after 27 iterations, which is shown in Figure 16.

We integrated the obtained results of the wall thickness rounding and the elastic modulus optimization. Finally, the joint optimization results of sizes and materials have been obtained, as shown in Table 5.

According to the parameters in Table 5, the wall thickness and material properties of the ten plates are assigned to the finite element model. The authors used the mass calculate module in the HyperMesh to measure the main rod plate mass. The mass values of all the plates are summed to obtain the final mass. And then the final mass was compared with that of the smart light pole before

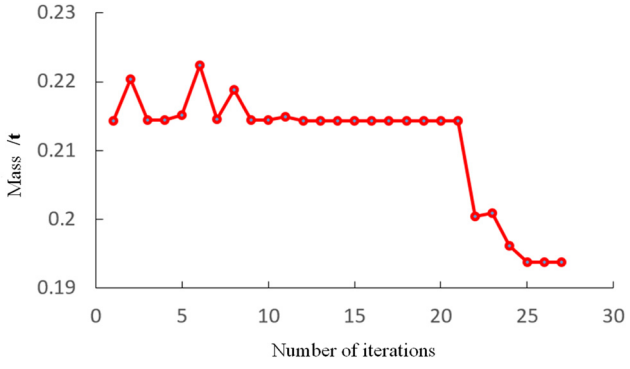

Figure 16: The iteration curve mass parameters.

Table 5: Joint optimization results of sizes and materials

Variable	Optimized thickness	Elastic modulus	Variable	Optimized thickness	Elastic modulus
Plate 1	3.5	213	Plate 6	2.5	213
Plate 2	3.5	210	Plate 7	2.5	210
Plate 3	3.0	213	Plate 8	2.5	210
Plate 4	3.0	213	Plate 9	2.5	210
Plate 5	3.0	213	Plate 10	4.5	206

Table 6: Results of the mass optimization

Name	Weight
Before	122.8 kg
After	107.5 kg
Optimization rate	14.2%

the optimization to obtain the optimization percentage. The mass optimization results are shown in Table 6.

4.3 Cost optimization of materials

To optimize the material cost of smart light poles, the candidate materials for optimization should meet the following three conditions: (1) Poisson's ratio and density should be similar to that of the raw material Q235B, (2) the cost should be low, and (3) the material should be common in industrial production. After data search and repeated screening, the metal materials that meet the above three conditions are finally determined to be Q235A, 60Mn, and Q345. The parameters are shown in Table 7.

Table 7: Parameters of the candidate materials for cost optimization

Material	Elastic modulus (GPa)	Poisson's rate	Density (T/m^3)	Yield strength (MPa)	Unit price (RMB)
Q235B	210	0.3	7.8	235	4.50
Q235A	213	0.3	7.8	235	4.48
60Mn	210	0.3	7.8	410	4.41
Q345	206	0.3	7.8	345	4.75

Statistical principles were used to combine different schemes; the cost of all combinations was calculated, and the optimal scheme for cost optimization was screened out. The materials of plate 2, plate 7, plate 8, and plate 9 all have two choices of Q235B and 60Mn, and the remaining design variables are only one material choice. According to statistical principles, there are a total of 24 cost optimization schemes. The specific schemes are shown in Table 8.

Table 8: Cost optimization schemes

Scheme	gan1	gan2	gan3	gan4	gan5	gan6	gan7	gan8	gan9	gan10	cost
1	**Q235A**	**60Mn**	**Q235A**	**Q235A**	**Q235A**	**Q235A**	**60Mn**	**60Mn**	**60Mn**	**Q345**	**481.45**
2	Q235A	Q235B	Q235A	Q235A	Q235A	Q235A	60Mn	60Mn	60Mn	Q345	481.48
3	Q235A	60Mn	Q235A	Q235A	Q235A	Q235A	60Mn	60Mn	Q235B	Q345	481.49
4	Q235A	60Mn	Q235A	Q235A	Q235A	Q235A	60Mn	Q235B	60Mn	Q345	481.49
5	Q235A	Q235B	Q235A	Q235A	Q235A	Q235A	60Mn	60Mn	Q235B	Q345	481.52
6	Q235A	Q235B	Q235A	Q235A	Q235A	Q235A	60Mn	Q235B	60Mn	Q345	481.52
7	Q235A	60Mn	Q235A	Q235A	Q235A	Q235A	60Mn	Q235B	Q235B	Q345	481.53
8	Q235A	Q235B	Q235A	Q235A	Q235A	Q235A	60Mn	Q235B	Q235B	Q345	481.56
9	Q235A	60Mn	Q235A	Q235A	Q235A	Q235A	Q235B	60Mn	60Mn	Q345	483.17
10	Q235A	Q235B	Q235A	Q235A	Q235A	Q235A	Q235B	60Mn	60Mn	Q345	483.20
11	Q235A	60Mn	Q235A	Q235A	Q235A	Q235A	Q235B	60Mn	Q235B	Q345	483.21
12	Q235A	60Mn	Q235A	Q235A	Q235A	Q235A	Q235B	Q235B	60Mn	Q345	483.21
13	Q235A	Q235B	Q235A	Q235A	Q235A	Q235A	Q235B	60Mn	Q235B	Q345	483.24
14	Q235A	Q235B	Q235A	Q235A	Q235A	Q235A	Q235B	Q235B	60Mn	Q345	483.24
15	Q235A	60Mn	Q235A	Q235A	Q235A	Q235A	Q235B	Q235B	Q235B	Q345	483.25
16	Q235A	Q235B	Q235A	Q235A	Q235A	Q235A	Q235B	Q235B	Q235B	Q345	483.28

Bold values are the best optimal scheme for cost optimization. The material of each plate and the total cost of this scheme are displayed.

Table 9: Parameters of the final optimization scheme

Name	Weight (kg)	Thickness (mm)	Elastic modulus (GPa)	Material	Unit price (RMB/kg)	Cost (RMB)
gan1	36.64	3.5	213	Q235A	4.48	164.15
gan2	0.279	3.5	210	60Mn	4.41	1.23
gan3	0.239	3.0	213	Q235A	4.48	1.07
gan4	4.06	3.0	213	Q235A	4.48	18.19
gan5	41.62	3.0	213	Q235A	4.48	186.46
gan6	0.62	2.5	213	Q235A	4.48	2.78
gan7	19.16	2.5	210	60Mn	4.41	84.50
gan8	0.366	2.5	210	60Mn	4.41	1.61
gan9	0.366	2.5	210	60Mn	4.41	1.61
gan10	4.178	4.0	206	Q345	4.75	19.85
Total	**107.53**					**481.45**

Table 10: Final optimization results of mass and cost

Name	Weight	Cost
Before	122.80 kg	552.60 RMB
After	107.53 kg	481.45 RMB
Optimization rate	14.2%	14.8%

It can be seen from Table 8 that the total cost of the main pole in the first scheme is the lowest, which is 481.45 RMB. The selected materials of Scheme 1 are summarized in Table 8, and the final optimization scheme with the best cost, size, and material for the optimal design is shown in Table 9.

After calculation, the cost of the smart light pole before optimization is 552.6 RMB, and the cost of the optimized smart light pole is 481.4 RMB. The optimization rate has reached 14.7%, which indicates that the cost optimization result is ideal.

4.4 Comprehensive performance verification of the optimized pole

According to results of the optimized design, we carried out the comprehensive performance verification on the optimized light pole. Considering that the distance between each mounted equipment and the mounting method have not changed, the electromagnetic interference affected by the radiation source is basically the same as that before optimization, which still complies with the electromagnetic compatibility design. After we used OptisTruct to deal with the optimized finite element model under static conditions, the results show that the optimized light pole's stress under the three extreme conditions all conform to the standard requirements. Besides, according to the optimized pole's dynamic characteristics verification, the overall modal performance remains basically unchanged. It also meets the standard requirements under the earthquake's full load condition.

Table 11: Before and after comparison of the comprehensive performance

Condition	Comprehensive performance	Before		After	
		Allowable value	Actual value	Allowable value	Actual value
Full load of typhoon	Maximum stress	235 MPa	88.506 MPa	235 MPa	112.144 MPa
	Maximum displacement	150 mm	12.339 mm	150 mm	14.270 mm
Full load of snow	Maximum stress	235 MPa	18.265 MPa	235 MPa	22.248 MPa
	Maximum displacement	150 mm	2.447 mm	150 mm	2.666 mm
Full load of wind and snow	Maximum stress	235 MPa	90.975 MPa	235 MPa	118.401 MPa
	Maximum displacement	150 mm	12.579	150 mm	14.502 mm
Full load of seismicity	Maximum stress	235 MPa	343.135 MPa	345 MPa	309.09 MPa
	Maximum displacement	150 mm	1.742 mm	150 mm	1.561 mm

4.5 Final result of optimization

Before optimization, the smart light pole's mass is 122.80 kg, and that after optimization is 107.53 kg. The total mass is reduced by 15.27 kg, and the optimization rate has reached 14.2%. The cost of the smart light pole before optimization is 552.60 RMB, and after optimization the cost is 481.45 RMB. The total cost has been reduced by 71.15 RMB, and the optimization rate has reached 14.7%. Therefore, the benefit of smart light pole optimization is obvious, as shown in Table 10. Through steady-state statics verification and structural dynamics verification on the optimized light poles, the authors make sure that the optimized scheme is rational and reliable. At last, the authors integrated all the verification results and compared them with the data before optimization. The final results are shown in Table 11.

5 Conclusions and future perspectives

In this study, the main work and conclusions obtained are as follows.

(1) Based on the software UG, the geometric model for the smart light pole was established and imported into the simulation software for pre-processing. Finally, the simulation model was obtained.
(2) Conducting steady-state static analysis, structural dynamics analysis, and electromagnetic interference analysis on smart light poles, the mechanical response of smart light poles under various working conditions was obtained. And that the electromagnetic interference between the various electronic devices mounted on the poles was clarified.
(3) Through the multi-parameter sensitivity analysis and the joint optimization of materials and sizes, the lightweight optimization of the smart light pole was realized. And according to the statistical principle, the lowest cost solution was selected. The cost optimization of the smart light pole was realized. Finally, the steady-state statics verification and structural dynamics verification were conducted. The optimized scheme is proved to be feasible.

The final results have certain engineering value for effectively integrating rod resources, designing smart light poles, and rationally arranging mounting equipment. Besides, this study can give a useful reference to CVIS design, especially for smart city construction, including the 5G material equipment [31–35].

Due to the weak diffraction and penetration capabilities of the 5G network to obstacles, a 5G base station needs to be deployed basically every 400 m. In order to cope with construction of such a large number of base stations, operators can use light poles in suitable locations as base station setting points to build communication base stations in distributed mode. In future work, based on the characteristics of 5G networks, the authors will further design the structure and materials of smart light poles to make them better serve 5G communications.

Funding information: This work was supported by the National Natural Science Foundation of China (Grant No. 51775565), Guangzhou Science and Technology Plan Project (No. 202007050004), and the Natural Science Foundation of Guangdong Province, China (2020A1515110160).

Author contributions: All authors have accepted responsibility for the entire content of this manuscript and approved its submission.

Conflict of interest: The authors state no conflict of interest.

References

[1] Pasolini G, Buratti C, Feltrin L. Smart city pilot projects using LoRa and IEEE802.15.4 technologies. Sensors. 2018;18(4):11–8. doi: 10.3390/s18041118.
[2] Sanchez SF, Cano OA. Smart regulation and efficiency energy system for street lighting with LoRa LPWAN. Sustain Cities Soc. 2021;70(3):102–12. doi: 10.1016/j.scs.2021.102912.
[3] Saidani NO, Sengan S, Thangavelu KD, Kumar SD, Setiawan R, Elangovan M, et al. Migrating from traditional grid to smart grid in smart cities promoted in developing country. Sustain Energy Technol Assess. 2021;45(9):78–81. doi: 10.1016/j.seta.2021.101125.
[4] Li W, Ban XG. Connected vehicle based traffic signal coordination. Engineering. 2020;6(11):14–28. doi: 10.1016/j.eng.2020.10.009.
[5] Tang Q, Yu T, Jen M. Finite element analysis for the damage detection of light pole structures. Proc SPIE 9437, Structural health monitoring and inspection of advanced materials, aerospace, and civil infrastructure 2015, vol 9437; 2015 April 1. p. 943711. doi: 10.1117/12.2075689.
[6] Daneshkhah AR, Menzemer CC. A finite element study of welded aluminum shoe-base light pole details. Eng Struct. 2019;198:109506. doi: 10.1016/j.engstruct.2019.109506. ISSN 0141-0296.
[7] Caracoglia L, Velazquez A. Experimental comparison of the dynamic performance for steel, aluminum and glass-fiber-

reinforced-polymer light poles. Eng Struct. 2008;30(4):1113–23. doi: 10.1016/j.engstruct.2007.07.024. ISSN 0141-0296.
[8] Siringoringo DM, Fujino Y, Nagasaki A, Matsubara T. Seismic performance evaluation of existing light poles on elevated highway bridges. Struct Infrastruct Eng. 2021;17(5):649–63. doi: 10.1080/15732479.2020.1760894.
[9] Hoisington D, Hamel S. Evaluating the behavior of anchor rod foundations for high-mast light poles using nonlinear finite-element analysis. J Struct Eng. 2016;142(9):04016047. doi: 10.1061/(ASCE)ST.1943-541X.0001495.
[10] Zajac P, Przybylek G. Lighting lamps in recreational areas – damage and prevention, testing and modelling. Eng Fail Anal. 2020;115:1–5. doi: 10.1016/j.engfailanal.2020.104693. ISSN 1350-6307.
[11] Soltani BA, Sabahi M, Babaei E, Pouladi J. Two-input boost converter for street-lighting applications. Comput Electr Eng. 2021;92(5):107–26. doi: 10.1016/j.compeleceng.2021.107126.
[12] Ai M, Wang P, Ma W. Research and application of smart streetlamp based on fuzzy control method. Proc Comput Sci. 2021;18(3):341–8. doi: 10.1016/j.procs.2021.02.069.
[13] Zhang X. Application of NB-IoT technology in urban lighting system. Int Core J Eng. 2020;6(4):246–51. doi: 10.6919/ICJE.202004_6(4).0036.
[14] Pal U, Mukhopadhyay G, Kumar BN, Bhattacharyya S. Electric pole failure: a safety concern. Eng Fail Anal. 2019;103(12):249–58. doi: 10.1016/j.engfailanal.2019.05.003.
[15] Juric J, Linden J. An empirical analysis of consumer resistance to smart-lighting products. Light Res Technol. 2019;51(4):489–512. doi: 10.1177/1477153518774080.
[16] Solari G, Pagnini LC. Gust buffeting and aeroelastic behaviour of poles and monotubular towers. J Fluids Struct. 1999;13(8):877–85. doi: 10.1006/jfls.1999.0240.
[17] Balagopal R, Rao NP, Rokade RP. Investigation on buckling behaviour of gfrp angle sections with bolted connections in lattice towers. J Inst Eng (India) Ser A. 2020;101(2):135–46. doi: 10.1007/s40030-020-00432-w.
[18] Sun MQ, Liu QP, Li ZQ, Wang E. Electrical emission in mortar under low compressive loading. Cem Concr Res. 2002;32(1):47–50. doi: 10.1016/S0008-8846(01)00627-5.
[19] Furlane A, Gomes HM, Almeida F. Design optimization of tapered steel wind turbine towers by QPSO algorithm. Int J Steel Struct. 2020;20(2):112–23. doi: 10.1007/s13296-020-00389-3.
[20] Ahmad F, Kumar P, Patil PP, Kumar V. Design and modal analysis of a quadcopter propeller through finite element analysis. Mater Today Proc. 2021;1:1–7. doi: 10.1016/j.matpr.2020.12.457. ISSN 2214-7853.
[21] Peng T, Guo Z. A new design strategy for seismic safety in super earthquakes of continuous girder bridges. Measurement. 2020;163:108000. doi: 10.1016/j.measurement.2020.108000. ISSN 0263-2241.
[22] Lu D, Ma C, Du X, Wang X. A new method for the evaluation of the ultimate seismic capacity of rectangular underground structures. Soil Dyn Earthq Eng. 2019;126:105776. doi: 10.1016/j.soildyn.2019.105776. ISSN 0267-7261.
[23] Wang X. Optimized design for an electromagnetic shielding shelter. Firepower Control Radar Tech. 2006;35(3):49–52. doi: 10.19472/j.cnki.1008-8652.2006.01.013.
[24] Shivakumara BS, Sridhar V. Study of vibration and its effect on health of the motorcycle rider. Online J Health Allied Sci. 2010;1(5):1–4.
[25] Chen H, Yang C, Deng K, Zhou N, Wu H. Multi-objective optimization of the hybrid wind/solar/fuel cell distributed generation system using hammersley sequence sampling. Int J Hydrog Energy. 2017;42(12):7836–46. doi: 10.1016/j.ijhydene.2017.01.202. ISSN 0360-3199.
[26] Xu X, Chen XB, Liu Z, Xu Y, Zhang Y. Reliability-based design for lightweight vehicle structures with uncertain manufacturing accuracy. Appl Math Model. 2021;95(11):9–19. doi: 10.1016/j.apm.2021.01.047.
[27] Sun Q, Guo Z, Chen W, Yu Y, Wang Z, Guo J, et al. Global sensitivity analysis of the main steam line break accident by using sampling methods and surrogate models. Ann Nucl Energy. 2021;150:107787. doi: 10.1016/j.anucene.2020.107787. ISSN 0306-4549.
[28] Shi H, Chen J, Hu L, Geng S, Zhang T, Feng Y. Multi-parameter sensitivity analysis on thermal characteristics of stratospheric airship. Case Stud Therm Eng. 2021;25:100902. doi: 10.1016/j.csite.2021.100902. ISSN 2214-157X.
[29] Hanna M, Schwenke J, Schwede LN, Laukotka F, Krause D. Model-based application of the methodical process for modular lightweight design of aircraft cabins. Proc CIRP. 2021;100:637–42. doi: 10.1016/j.procir.2021.05.136. ISSN 2212-8271.
[30] Zhang RH, He ZC, Wang HW, You F, Li KN. Study on self-tuning tyre friction control for developing main-servo loop integrated chassis control system. IEEE Access. 2017;5:6649–60. doi: 10.1109/ACCESS.2017.2669263.
[31] Fu J, Liu Q, Ma Y, Zhang Z. A comparative study on energy absorption of flat sides and corner elements in CFRP square tube under axial compression. Thin-Wall Struct. 2021;166:108080. doi: 10.1016/j.tws.2021.108080.
[32] Fu J, Liu Q, Liufu K, Deng Y, Fang J, Li Q. Design of bionic-bamboo thin-walled structures for energy absorption. Thin-Wall Struct. 2019;135:400–13. doi: 10.1016/j.tws.2018.10.003.
[33] Liu Q, Liufua KM, Cuia Z, Li J, Fang J, Li Q. Multiobjective optimization of perforated square CFRP tubes for crashworthiness. Thin-Wall Struct. 2020;149:106628. doi: 10.1016/j.tws.2020.106628.
[34] Chen X, Lu J, Zhao J, Qu Z, Yang Y, Xian J. Traffic flow prediction at varied time scales via ensemble empirical mode decomposition and artificial neural network. Sustainability. 2020;12(9):3678. doi: 10.3390/su12093678.
[35] Chen X, Li Z, Yang Y, Qi L, Ke R. High-resolution vehicle trajectory extraction and denoising from aerial videos. IEEE Trans Intell Transp Syst. 2021;22(5):3190–202. doi: 10.1109/TITS.2020.3003782.